

HEAM : Hashed Embedding Acceleration using Processing-In-Memory

Youngsuk Kim, Hyuk-Jae Lee and Chae Eun Rhee

Abstract

In today’s data centers, personalized recommendation systems face challenges such as the need for large memory capacity and high bandwidth, especially when performing embedding operations. Previous approaches have relied on DIMM-based near-memory processing techniques or introduced 3D-stacked DRAM to address memory-bound issues and expand memory bandwidth. However, these solutions fall short when dealing with the expanding size of personalized recommendation systems. Recommendation models have grown to sizes exceeding tens of terabytes, making them challenging to run efficiently on traditional single-node inference servers. Although various algorithmic methods have been proposed to reduce embedding table capacity, they often result in increased memory access or inefficient utilization of memory resources.

This paper introduces HEAM, a heterogeneous memory architecture that integrates 3D-stacked DRAM with DIMM to accelerate recommendation systems in which compositional embedding is utilized—a technique aimed at reducing the size of embedding tables. The architecture is organized into a three-tier memory hierarchy consisting of conventional DIMM, 3D-stacked DRAM with a base die-level Processing-In-Memory (PIM), and a bank group-level PIM incorporating a Look-Up Table. This setup is specifically designed to accommodate the unique aspects of compositional embedding, such as temporal locality and embedding table capacity. This design effectively reduces bank access, improves access efficiency, and enhances overall throughput, resulting in 6.3× speedup and 58.9% energy savings compared to the baseline.

1 Introduction

Personalized recommendation serves as an important technology of various companies such as Meta [1], YouTube [2] and Netflix [3]. In recent days, deep learning-based recommendation systems have emerged as a pivotal technology for improving the accuracy of predicting user-preferred content, thereby contributing to enhanced profitability for these companies. These advanced recommendation systems currently contribute substantially to the computational workload of the data center. Recent reports indicate that approximately 80% of data center resources are dedicated to the inference process of recommendation systems [4].

In order to offer personalized item suggestions to individual users, recommendation models rely on two distinct types of input: Dense features and Sparse features. Dense

features represent individual user information as floating-point vectors, which are fed into the multi-layer perceptron (MLP) layers. Sparse features, on the other hand, encompass item-specific information and are processed through an embedding operation. The intermediate outputs generated at each stage are subsequently interacted with each other, serving as input for the top MLP layers. These top MLP layers then produce a click-through-rate (CTR) prediction, estimating the likelihood of a user clicking on the recommended item.

In large-scale data centers that extensively utilize embeddings, the embedding operation often becomes the primary factor influencing overall system performance. This stems mainly from the operation’s tendency to exhibit sparse and irregular memory access patterns. As a result, these memory-bound operations place significant constraints on traditional data center infrastructures [5], and this challenge continues to grow with the scale, as depicted in Figure 1.

To tackle this challenge, recent efforts have concentrated on designing memory systems tailored to embedding operation [6], [7], [8], [9], [10], [11]. Approaches like TensorDIMM [6] and RecNMP [7] have explored the effectiveness of incorporating near-memory-processing (NMP) to alleviate the memory-bound nature by accelerating embedding operations directly within off-chip memory. These architectural solutions expedite the gather-and-reduce (GNR) process of embedding operations by deploying processing units in each rank of Dual Inline Memory Module (DIMM). This approach effectively harnesses the internal memory bandwidth, which is further amplified by the number of ranks in the memory channel. TRiM [8] and SPACE [9] followed a similar NMP structure while introducing other modifications to memory architecture. TRiM employed bank group-level PIM within the DRAM device, while SPACE utilized High Bandwidth Memory (HBM) as a Dynamic Random Access Memory (DRAM) cache.

On the other hand, personalized recommendation models are currently expanding in its size. According to RecShard [12], the memory capacity requirement of the Deep Learning Recommendation Model (DLRM) has been enlarged to the 16 times during 2017 to 2021, as shown in Figure 1. The growth of the model is due to the fact that more sparse features attribute to better model quality [12], [13]. However, The model operating on the inference server [5], [14], [15], [16] is significantly smaller in scale compared to the training model [12], [13]. Therefore, there exists a significant gap between the training model size and inference model size. Serving the

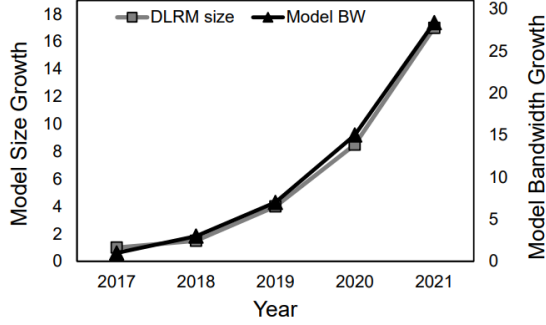


Figure 1. Model size and bandwidth growth of DLRM. (Reproduction from RecShard [12])

inference with multi-node server or introducing Solid-State-Drivers (SSDs) could be a possible solution, but it comes at the cost of synchronization and vulnerability to failures for the multi-node server case, and the SSDs have a negative impact on execution time [14], [17]. Therefore, exploring an alternative approach is essential to optimize model inference without encountering these drawbacks. Prior works took algorithmic approaches to reduce the embedding table size [18], [19], [20], [21]. While these techniques have successfully reduced the size of the embedding table, their work has been done at the cost of imposition of much heavier burden to the memory bandwidth or inefficient memory capacity management.

We propose HEAM, a specialized memory architecture integrated with PIM technology, designed to accelerate the inference process of compositional embedding [18]. Compositional embedding employs a simple double-hashing technique for quotient (Q) and remainder (R) tables to acquire the base embedding data. Consequently, this approach produces vectors with consistent dimensions across all data points, streamlining their efficient utilization in memory. Nevertheless, the double memory access necessary for double hashing amplifies the memory-bound characteristics. HEAM introduces a three-tiered memory hierarchy consisting of DIMM, HBM, and a lookup table (LUT). HBM is incorporated with base-die PIM (bd-PIM), while LUT serves as the storage space within bank-group PIM (bg-PIM), thereby enhancing memory parallelism. The GnR processing in PIM can further reduce memory bandwidth requirements. This design is based on the following observations. Similar to original embedding, Q table exhibits high temporal locality characteristic within a small portion of entire embedding vector. Therefore, HEAM leverages HBM and DIMM to exploit this temporal locality. Notably, the R table, in particular, has a very small size and demonstrates a remarkably high temporal locality. Hence, we utilize an LUT within bg-PIM to store the entire R table. By addressing the memory bandwidth challenges associated with compositional embedding, HEAM effectively

reduces the size of the embedding tables while simultaneously satisfying the requirements for memory bandwidth. This capability enables the execution of large models on a single-node server at a high processing speed. The primary contributions of our work can be summarized as follows:

- To the best of our knowledge, HEAM is the first work to address both the large model size problem and the memory-bound issue of the DLRM. HEAM successfully tackles both issues by designing a specialized hardware for compositional embedding.
- We propose an allocation strategy for each hash table in compositional embedding. By distinguishing storage space for each table based on the analysis of their unique characteristics, HEAM achieves additional gains in bandwidth.
- We design a two-level PIM within HBM, specifically tailored for compositional embedding. This enables HEAM to expand into a three-tiered memory system, incorporating DIMM, HBM, and the LUT within PIM, thus effectively enhancing memory parallelism.

2 Background

2.1 Personalized Recommendation System

Recommendation System Overview. Among the various personalized recommendation models employed by diverse companies, DLRM stands out as one of the prominent recommendation system models. In the DLRM framework, inputs are categorized into two groups: dense features and sparse features. Dense features correspond to user information expressed as floating-point values, while sparse features facilitate access to items by transforming them into embedding vectors that encapsulate item-specific features. Figure 2 provides an illustration of the DLRM architecture. The bottom-mlp takes dense features as inputs, while the embedding lookup process handles sparse features. The embedding lookup operation gathers individual embedding vectors from multiple embedding tables, generating a single reduced vector. This reduced embedding vector is subsequently concatenated with the outcome of the bottom-mlp through a feature interaction layer. The resulting combined representation is then fed into the top-mlp. Once the top-mlp completes its calculations, the final outcome, CTR, is generated.

Challenges in Recommendation System Inference. The performance of the recommendation system is constrained by the memory-bound nature of the embedding operation. The irregular access patterns of embedding vectors, combined with the extensive size of the embedding table that surpasses the cache storage capacity on the host side, necessitate the frequent look-up of embedding vectors from the off-chip memory system. This frequent access to main memory leads to higher latency for the embedding operation compared to that of the bottom-mlp [9], classifying the model as memory-bound.

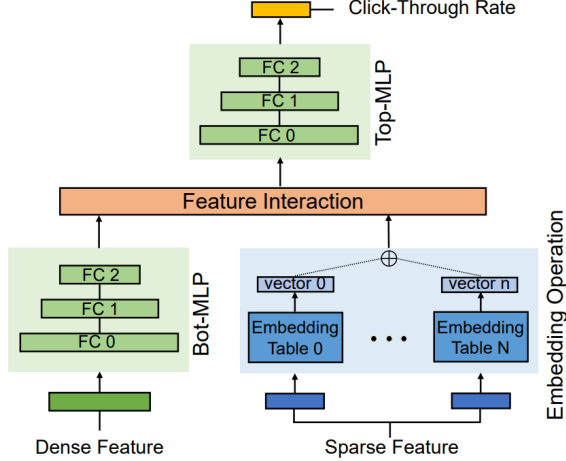


Figure 2. DLRM architecture

Recently, recommendation models have been trending towards incorporating increasingly large-sized embedding tables, with their scale growing year by year [12]. Nowadays, industry-scale DLRM implementations require substantial memory resources, often reaching sizes of up to tens of terabytes, a significant portion of which is dedicated to housing embedding tables [14], [5]. Given that the quality of the model is closely linked to the size of these embedding tables, there is a strong incentive to utilize as large embedding tables as possible in production. However, the practical utilization of such large models is constrained by physical limitations, as the memory size of a single-node server is restricted by the available slots within the server.

2.2 Algorithms for Reducing Embedding Data Size

Algorithms Overview. Table 1 presents a comparison of various algorithmic approaches for the reduction of embedding table sizes, including their respective compression rates, accuracy relative to the original data, and operational characteristics. These methods can be categorized into three groups. The first group employs parameter sharing techniques, utilizing hashing methods that map certain subsets of embedding vectors to the same vector. Examples of parameter sharing methods include the hashing trick [22] and compositional embedding [18]. Conversely, the second group focuses on eliminating redundancy within the embedding dimensions themselves. In approaches like Mixed-Dimension-Embedding [19] and OptEmbed [21], embeddings that have minimal impact on the output are resized to a smaller dimension. The third group, instead of storing embeddings as data, generates them from input indices using compute-intensive operations like MLP. Notable works following this approach include TT-Rec [20] and Deep-Hash-Encoding [23].

The first group offers advantages in terms of memory efficiency. This group produces vectors with uniform dimensions as the algorithm’s output, promoting efficient utilization of memory capacity and accommodating memory system bursts effectively. Another benefit is the relatively low computational complexity of hash functions. However, the drawback is that the accuracy tends to lag behind the baseline due to the semantic overlap among non-relevant embeddings. Furthermore, the degree of compression achieved is relatively modest. The second and third groups attain high compression rate along with the better model accuracy than the baseline. In the second group, however, efficient use of memory resource is relatively hard since the output vectors vary in its dimension. Finally, the last group transforms the target model into compute-bound application, which is far apart from the memory perspective, contrast to other groups which are memory-bound applications. The second and third groups achieve a substantial compression rate while also delivering improved model accuracy compared to the baseline. In the second group, however, efficient utilization of memory resources is relatively challenging because the output vectors exhibit varying dimensions. On the other hand, the third group transforms the target model into a compute-bound application, diverging significantly from the memory-oriented perspective of the other groups, which are memory-bound applications.

Table 1. Comparison of embedding table reduction schemes.

Method	Compression	AUC	BW bound	Mem. friendly
Hashing [22]	Low	Much Lower	Memory	✓
QR [18]	Moderate	Lower	Memory	✓
MDE [19]	Moderate	Better	Memory	✗
OptEmbed [21]	High	Better	Memory	✗
TT-Rec [20]	High	Better	Compute	✗
DHE [23]	High	Better	Compute	✗

Compositional Embedding. Compositional embedding employs two types of hash functions, effectively partitioning the original embedding table into two smaller tables, as depicted in Figure 3 (a). These hash functions include the quotient operation and remainder operation. Embeddings that yield the same quotient result are mapped to corresponding vectors in the table generated by the quotient function (Q table). In contrast, embeddings with identical remainder results are directed to the same vector within the other hash table (R table). The total table size is typically reduced by a factor approximately equal to the inverse of the hash collision, with the R table size being usually negligible in comparison to that of the Q table. The R table size corresponds to the hash collision, whereas the Q table size is equivalent to the original table size divided by the hash collision. To process the embedding operation, it is necessary to reconstruct the original embedding. This is accomplished by performing

straightforward mathematical operations on the vectors extracted from each table. The overall scheme is illustrated in Figure 3 (b).

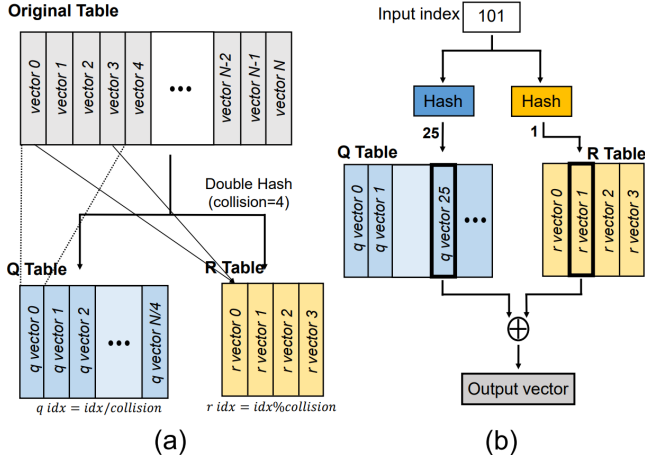


Figure 3. Compositional embedding overview. (a) Double hashing process (b) Embedding vector reconstruction process

2.3 NMP/PIM Designs for Recommendation System

To meet the memory bandwidth requirements of recommendation systems, recent studies have introduced NMP units within the DRAM architecture. Specifically, these approaches have incorporated multiple DIMMs with NMP units situated within their DIMM/Rank configurations, effectively exploiting DIMM/Rank-level parallelism [6], [7] to achieve increased throughput. TRiM [8] focused on the tree topological structure of the DRAM’s data path, further enhancing parallelism by integrating PIM units within each bank group. In pursuit of additional speedup, the aforementioned designs have leveraged the long-tail distribution of embeddings, where a small subset of embeddings is frequently reused. This has been accomplished by incorporating a cache within the buffer chip [7] or implementing load-balancing techniques with the assistance of the memory controller [8].

While it is possible to increase the throughput of the embedding operation by incorporating more DIMMs with NMP designs from previous approaches, this may lead to inefficiencies in terms of power consumption [9]. To address this challenge, SPACE [9] introduced a heterogeneous memory system that combines HBM and DIMMs, with HBM functioning as a DRAM cache. Additionally, SPACE exploited the reduced locality of embedding vectors and the long-tail distribution of embedding vectors to achieve significantly higher throughput. In summary, achieving high performance in recommendation systems relies on core techniques that involve exploiting parallelism within the main memory and capitalizing on the long-tail distribution of embedding vectors.

3 Analysis on Compositional Embedding

As shown in Section 2.2, compositional embedding exhibits several advantages over other previously proposed schemes concerning the memory system. While alternative methods may yield better model prediction quality and higher compression rates, the nature of the output data poses challenges for the memory system when supporting the embedding operation. Consequently, we have selected compositional embedding as the target algorithm. In this section, we offer an in-depth analysis of the characteristics of compositional embedding.

3.1 Impact on DLRM Throughput

Compositional embedding further intensifies the memory-bound characteristics of the model by doubling the overall number of accesses to main memory. This is because generating input vectors for the model necessitates accessing two hash tables. Figure 4 (a) presents a comparison of the execution times for embedding operations on HBM and DIMM between the original model and the model with compositional embedding applied. The results indicate that compositional embedding leads to a 25% longer execution time on HBM and a 40% longer execution time on DIMM. Although the decrease in throughput is less pronounced on HBM due to its significantly higher number of channels compared to DIMM, it is evident that employing the compositional embedding results in increased memory access. This underlines the need for higher bandwidth than what traditional memory systems can provide.

3.2 Temporal and Spatial Locality

To investigate the locality characteristics in compositional embedding, we simulated cache behavior with embedding traces from criteo-kaggle-dataset [24]. A 4-way set associative cache is used during experiment. Note that MLP weights are not included during the simulation, thereby producing high cache hit rate of embeddings.

Temporal Locality. To find out the presence of temporal locality, we followed the method used in RecNMP [7]. We increased cache size from 1MB to 4MB and examined the difference in hit rate of random traces and traces generated from criteo dataset [24], [25] with compositional embedding applied, as depicted in Figure 4 (b). Total hit rate of compositional embedding is summation of Q table and R table hit rate, which is much higher than that of the random traces. This result implies the temporal locality characteristics on double-hashed embeddings. Although hit rate of Q table is slightly smaller than R table, it is still much higher compared to random traces, indicating strong temporal locality of Q table embeddings which resembles to original table locality characteristics examined in prior works [7], [9]. This is due to the similar long-tail distribution between the original and the Q table, as illustrated in the Figure 5. According to the

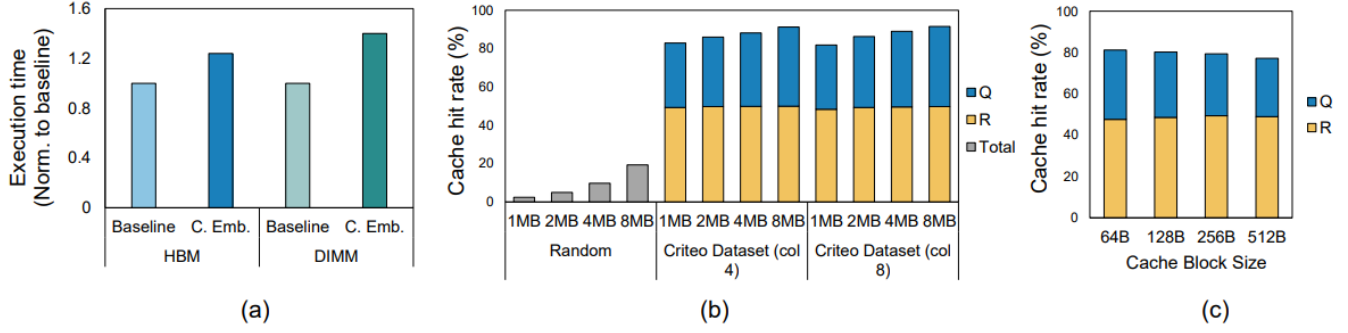


Figure 4. Compositional Embedding Analysis (a) Execution time comparison between original DLRM and compositional-embedding-applied DLRM (b) Verifying temporal locality by increasing cache size from 1MB to 4MB with vector length of 64B (c) Spatial locality by increasing cacheline size from 64B to 512B where cache size is fixed to 1MB with vector length of 64B

Figure 5 (a), a small subset of total embeddings take the majority of the access. We refer to this subset as *hot vectors*. As the number of hot vectors are small, they are sparse across embedding table. When quotient hashing maps consecutive embeddings to the same embedding, hot vectors tend to remain as hot vectors, since access rate of Q table embedding is identical to the access rate summation of consecutive embeddings that are mapped to that Q table embedding. Therefore, long-tail distribution remains as shown in Figure 5 (b).

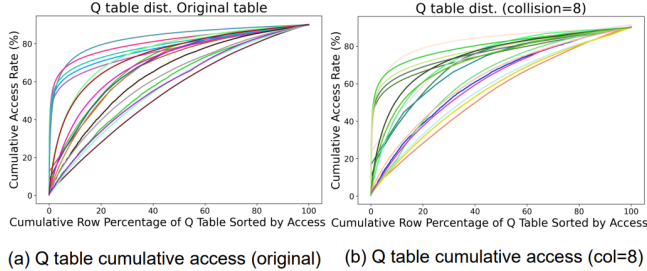


Figure 5. Cumulative access distribution of tables. (a) Original table (b) Q table with hash collision=8.

As depicted in the Figure 4 (b), R table cache hit rate occupies fixed, high portion of the total hit rate across all the cache size. This indicates each vector inside R table presents high temporal locality. The primary reason for this intensive temporal locality is relatively small amount of R table embeddings compared to the Q table embeddings even though total access to R table is identical to that of the Q table as both tables must be concurrently accessed to construct the input embedding. As a result, total access to the R table is concentrated on the small amount of embeddings, thereby increasing temporal locality to a significant portion. It is worth noting that R table embeddings displays uniform distribution as illustrated in Figure 6, which is more intensified when hash collision is low as illustrated in the figure. Since the hot vectors are randomly wide spread across the embedding table, the remainder hash function maps hot vectors

randomly to the R table embeddings. Coupled with the fact that R table exhibits high temporal locality, uniform access distribution of R table embeddings indicates that all the R vectors are hot vectors.

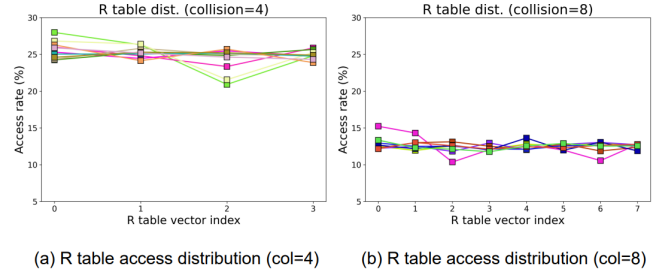


Figure 6. R table access distribution of 10 embedding tables. (a) Distribution with collision of 4 (b) Distribution with hash collision of 8. All embeddings have similar access distribution.

Spatial Locality. The simulation on spatial locality was conducted by measuring hit rate of 64B length vector on 1MB cache, varying the cacheline size from 64B to 512B on 1MB cache, again following the method used in [7]. Results are shown in Figure 4 (c). The observation shows that Q table cache hit rate decreases slightly, indicating little spatial locality. However, the R table cache hit rate implies that a mild level of spatial locality exists since the overall cache hit rate is stable, even though increasing cacheline size diminishes the effect of temporal locality, suggesting the existence of spatial locality. Despite the presence of R table spatial locality, it is challenging to benefit from such characteristic as its impact is minimal. Furthermore, the embedding dimension exceeds traditional cacheline size, as vector length utilized in recommendation system typically ranges from 64B to 512B. Fetching multiple R table vectors within a cacheline is impossible although R table vectors might be placed next to each other.

3.3 Opportunities for PIM Support

The above assessments suggest that enhanced throughput support is necessary for running compositional embedding during the inference stage. Inspired by the previous works that utilize NMP/PIM to extend the bandwidth [6], [7], [8], we conclude that employing PIM is an effective solution for addressing the memory-bound characteristic of compositional embedding. There are two attributes of compositional embedding that makes the usage of PIM more effective. First, as described in Section 2.2, the data arrangement is suitable enough to employ the PIM architecture. This is due to the uniformity in vector dimensions, which ensures efficient use of memory capacity and consistency in the total DRAM burst needed for each vector. Second, unique features of the R table vectors, high temporal locality and its uniform memory access distribution, could be efficiently exploited by extending PIM design to further increase the throughput. Integrated with heterogeneous system consisting of DIMM and HBM with base die PIM, utilization of PIM is an effective design for supporting compositional embedding.

4 HEAM Architecture

4.1 Architecture Overview

We propose HEAM, a specialized memory system designed to enhance the bandwidth of DLRM when compositional embedding is employed. The overall architecture is depicted in Figure 7. As illustrated in Figure 7 (a), the HEAM system incorporates a heterogeneous memory architecture that comprises HBM and DIMM, which addresses the memory-bound nature to some extent by offloading frequently accessed vectors to HBM. Nonetheless, it's important to note that the overall memory access demands for the embedding operation double when compositional embedding is employed. As a result, depending solely on HBM remains insufficient in terms of achieving the required throughput.

To tackle this problem, we design a two-level PIM system within the HBM to enhance the throughput by utilizing in-memory parallelism, thereby providing additional bandwidth support for the embedding operation. In Figure 7 (b), the first-level processing unit is located on the base die of the HBM, whereas the second-level processing units are located inside each bank group. These processing units are referred to as bd-PIM and bg-PIM, named based on their respective locations. Within these PIMs, the embedding operation is processed in a two-stage partial addition fashion. Initially, each bg-PIM collects Q embeddings and their corresponding R embeddings from its dedicated bank group. Local addition is performed inside each bg-PIM on the collected embedding vectors, generating partial results. Once all bg-PIMs complete their respective operations, all the reduced vectors are forwarded to the bd-PIM. The same operation is carried out within the bd-PIM for each set of partial results, resulting in the final output, which is delivered to the host processor.

Figure 8 (b) depicts the PIM architecture of bg-PIM. The system inside bg-PIM is equipped with an instruction register, an instruction decoder and a Multiply-and-Accumulate (MAC) unit. Additionally, LUT is integrated inside each bg-PIM to leverage the temporal locality of the R table described in Section 3.2. Therefore, the access to R embedding vectors are always directed to the LUT, resulting decrease of the total bank access. To address the load imbalance issue, HEAM employ batching of 4 embedding operations, following technique utilized in RecNMP [7]. To avoid introducing too much area overhead into bank groups, we use up to 4 batch in our system. The bd-PIM receives partial sums delivered from bg-PIM and process final GnR operation as illustrated in Figure 8 (a). Note that the architecture of the bd-PIM is similar to that of the previous works.

4.2 Hash Table Allocation Strategy

To mitigate the challenge of the double memory access problem associated with compositional embedding, we store the R and Q tables in memory in different ways. This is based on that the data access patterns for each table are distinct and exhibit significant variation from one another. Consequently, we ensure more efficient use of memory system resources. As these data access patterns are established after the training phase, we collect this distribution information prior to entering the inference stage. This additional process incurs just minimal overhead, as demonstrated in previous studies such as [7] and [9].

Mapping Scheme for Q table. As the Q table typically exhibits a long-tail distribution similar to that of the original embedding table, we leverage an approach inspired by SPACE [9] to exploit the Q table's characteristics. Embedding data with high temporal locality is offloaded to HBM, while the remaining embedding data are stored in DIMMs. The proportion of data to be offloaded to HBM is determined based on the bandwidth ratio between HBM and DIMM. This strategy, which involves gathering embedding data with high locality from HBM and fetching the rest from DIMMs, enhances the overall parallelism between the different memory types.

Mapping Scheme for R table. As described in Section 3.2, access to the R table is repeatedly conducted for a very limited set of data, consequently, all the data within the R table exhibits extremely high temporal locality. Based on the observation, HEAM stores all the R table embeddings inside the LUT that is located in each bg-PIM. Inside the bg-PIM, R embeddings are directed to the LUT as depicted in the Figure 8 (b). As a result, the number of bank accesses in compositional embedding is reduced by half, making the total number of accesses equivalent to that of the original model. Additionally, given the fact that the R embeddings follow a uniform distribution, load balance between LUT entries is achieved automatically. The total area overhead of LUT is minimal, as the number of entries required within

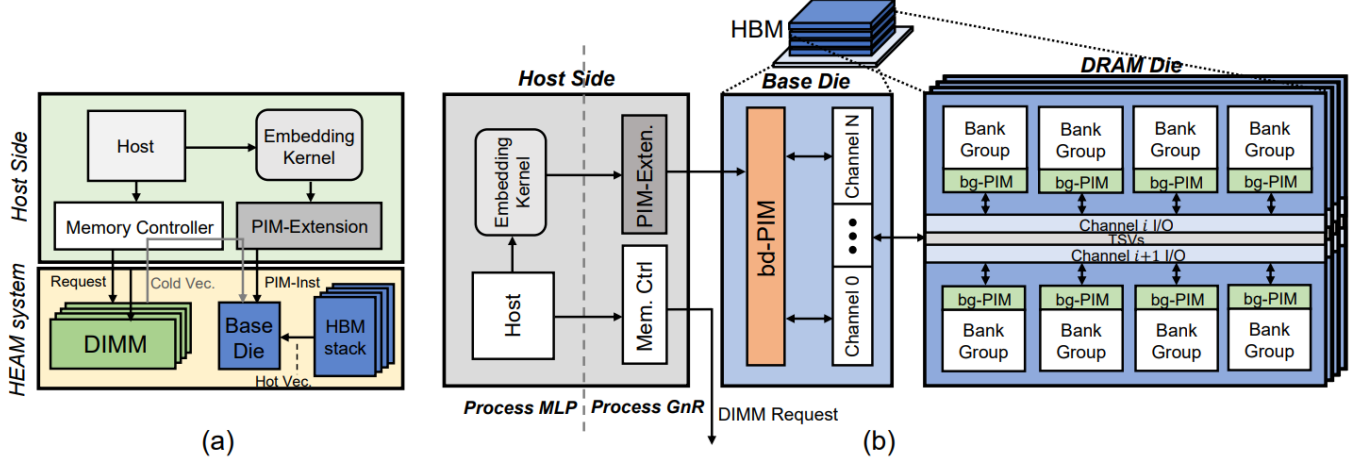


Figure 7. HEAM architecture. (a) Overview of HEAM architecture, (b) 2-level PIM system in HBM

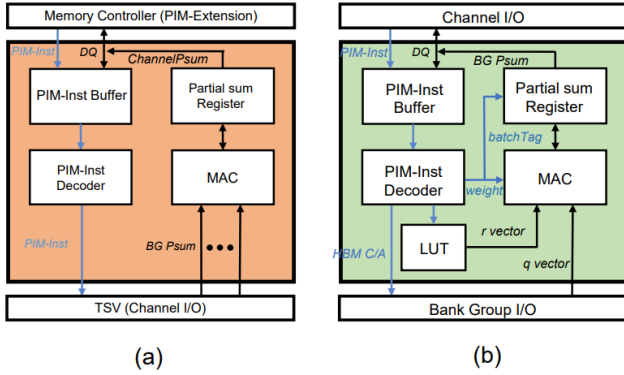


Figure 8. PIM architectures. (a) bd-PIM, (b) bg-PIM

the LUT is typically small considering the hash collision is usually set as a value less than 100. As we employ simple addition for input embedding reconstruction operation, we evenly allocate all the R table across all LUTs in a random fashion, without forcing Q table and R table to be placed within the same bank group.

While bd-PIM could be considered for LUT placement, bg-PIM offers distinct advantages. Placing LUT within bd-PIM, which requires housing all R tables in the base die, leads to substantial area overhead. The additional space needed for LUT placement on the base die is constrained by the presence of existing logic elements. This limitation becomes increasingly challenging as the number of tables, the frequency of hash collisions, and the sizes of the vectors grow. For instance, a model with 100 embedding tables, a hash collision of 50, and a vector size of 512B would require an additional 2.44MB of area on the base die for the R table (100 tables \times 512B \times 50 collision). On the other hand, storing the R table in bg-PIM distributes these tables across the four dies of HBM. Each PIM in its respective bank group only requires an additional 80KB of area. Given that the typical

bank group size in HBM is around 64MB, this area overhead is manageable. Moreover, this configuration can accommodate expansions in hash collision, total tables, and vector dimensions to a certain extent, making it a more scalable solution.

4.3 Hash Collision Value for HEAM System

As the Q table exhibits similar locality characteristics to the original, the advantage of heterogeneous memory systems described in SPACE [9] is applicable to compositional embedding. Moreover, to diminish the hash collision value, HBM-only scenario incurs redundant bandwidth since it needs to introduce additional stacks to increase capacity, while the heterogeneous system achieves the same hash collision without extra bandwidth. In order to fully reap the maximum bandwidth, each memory request ratio has to be equal to the bandwidth ratio, as displayed in the equation 1.

$$\frac{Request_{HBM}}{Request_{DIMM}} = \frac{BW_{HBM}}{BW_{DIMM}} \quad (1)$$

When HBM bandwidth is expanded with PIM, the overall HBM request should be enlarged to meet the above equation, forcing additional data offloading to the HBM. This might demand higher hash collision which leads to decrease in model quality. However, long tail distribution compensates such problem as increasing cumulative request of HBM requires small amount of additional data. Therefore, there is no need to introduce extra hash collision in order to meet the bandwidth demand.

4.4 PIM Instructions and the Execution Flow

PIM Instructions. HEAM leverages the PIM instruction to deliver embedding operation informations to each bg-PIM, following RecNMP [7] and TRiM [8]. Total width of a single PIM instruction is 84 bits. The *opcode* (3-bit) specifies the operation type that bd-PIM and bg-PIM should take into

action for GnR operation. The *target address* (34-bit) denotes the start address of the PIM-Inst to read from the bank group. *nRD* (4-bit) indicates the vector size. The *weight* (32-bit) delivers weight information for weighted sum. *transfer* (1-bit) determines whether the partial sum are complete and ready to deliver. The *skewed-cycle* (6-bit) instructs bg-PIM the time that PIM instruction should be decoded after being delivered to the bg-PIM. The *batchTag* (2-bit) is the assigned batch of the PIM instruction.

Execution Flow. To run the PIM system, it is essential for the memory controller to deliver PIM instructions to the memory system properly. Like prior works [7], [8], [9], HEAM offers an embedding operation driver that extends the current memory controller. The driver receives embedding operation from the host, construct PIM-instructions, and offloads it to the NMP at the HBM. When HBM is used as a DRAM cache inside heterogeneous memory system, a mapping of data is required to be stored inside the memory controller in order to direct each of the commands to the proper memory system. To support this, embeddings are mapped with direct mapping method. With the aid of the direct mapping method, the memory controller could send PIM-instruction and DDR4 command to each memory by adopting the method used in SPACE [9]. To avoid the cache coherence issues, we allocate memory space dedicated to HEAM as uncachable. Additionally, to cope with the command/address (C/A) bandwidth overhead issue addressed before [8], we follow the method or prior works that utilize data (DQ) pins to deliver a number of instructions to bg-PIMs within short cycle. Specifically, we utilize 14 C/A pins with 256 bit wide DQ pins to transfer up to 3 PIM instructions in a single cycle. Due to the abundant HBM DQ pins, HEAM successfully addresses the C/A bandwidth overhead.

5 Experimental Setup

Simulation Methodology. We modified DRAMsim3 [26], a cycle-accurate memory simulator to implement and evaluate the performance of HEAM system. HBM2 x128 and DDR4-3200 x8 were utilized as base memory system for HEAM system and the baselines. Table 2 summarizes the memory system configuration utilized in our experiment. Within a single DDR4-3200 x8 device, 2 ranks were employed. To utilize the heterogeneous memory systems, HEAM make use of flat addressable method which has been continuously adopted in prior works on the same system configuration [9], [27], [28], [29]. We compare HEAM performance against previous NMP architectures, TensorDIMM [6], RecNMP [7], TRiM [8] and SPACE [9]. The traces of embedding operation were extracted from running the DLRM model which are fed into simulation framework.

In order to meet fair comparison, we treat all the embeddings within R table as hot vectors so that temporal locality utilization techniques proposed in prior works could be

maximally exploited. For instance, we mark every R table embeddings with *localityBit* when implementing RecNMP. For TRiM implementation, R table embeddings has the highest priority when participating in *hot entry profiling*. In this case, vectors counted from the front of q vectors that are ordered with highest locality takes participation in hot entry profiling after R table. To fairly measure performance of SPACE, *reduction locality* technique was employed, storing partial sums of hot vectors in the available space on HBM2.

Area and Power Consumption. To obtain area and the power of PIM units, bd-PIM and bg-PIM were synthesized using Synopsys Design Compiler with 45nm CMOS technology operating at 300MHz clock frequency. For the case of bg-PIM, the corresponding area was scaled to a 20nm DRAM processing. Area and the power of LUT used inside bg-PIM was estimated using CACTI [30].

Recommendation System Datasets. Obtaining sufficiently large dataset is crucial for our experiment as HBM2 capacity needs to be fully occupied even after compositional embedding is applied regarding the assumption of HEAM system. However, since datasets meeting such constraint is not publicly available, we utilize criteo datasets [24],[25] by setting its vector size large enough, 128B to 512B. Note that criteo-terabyte dataset [25] capacity is near 10 GB when the vector length is 64B.

Table 2. Memory System configurations

HBM2 x128 device	
Organizations	8 channels per 4-hi stack, 4 bank groups per channel
Timing parameters	tCL=14, tRP=14, tRCD=14, tCCD_S=1, tCCD_L=2, tBL=16
Clock frequency	1000MHz
DDR4-3200 x8 device	
Organizations	1 channel per DIMM, 2 ranks per channel, 4 bank groups per rank
Timing parameters	tCL=22, tRP=22, tRCD=22, tCCD_S=4, tCCD_L=8, tBL=8
Clock frequency	1600MHz

6 Evaluation Result

We evaluate the impact of HEAM’s design choices as the first step to analyze the effectiveness of each choice. We then compare the performance of HEAM with state-of-the-art NMP designs which targets the embedding operation. Additionally, hardware overhead introduced to the overall system for HEAM architecture support is analyzed. We assess the limitations of compositional embedding to explore the boundary in terms of compositional embedding could be applied to our system in terms of preserving model quality.

6.1 Performance Impact of Design Optimizations

Following TRiM [8], we demonstrate the impact of each design optimization choice on the speedup performance. Figure 9 displays the performance improvements when design optimizations are gradually incorporated in HEAM system. The baseline is the execution speed of HBM2 in conjunction with bd-PIM. The first scenario is *HEAM-BG*, where bg-PIM without LUT is located in each bank group. The following scheme is *CA compression*, when command address compression is applied to HEAM-BG scenario. *Batching* corresponds to when batching technique is applied to the HEAM system. Finally, *LUT* scheme adds LUT to Batching scenario, reducing direct access to the bank of R table. Applying all the optimization techniques achieves 2.8 \times higher result compared to the baseline when vector size is 512B. HEAM-BG enhance the performance by 10% compared to the baseline. CA compression enhances 14% of the performance as the CA bandwidth overhead is mitigated, by both utilizing CA pin and DQ pin of HBM2. Batching scheme gains 86% of additional speedup by reducing load imbalance issue and satisfying high demand of pooling size of bg-PIM utilized inside HBM2. The root of the performance benefit of Batching lies in pulling up the potential of bank group level parallelism. Finally, 19% more speedup is acquired when it comes to LUT scenario, as it reduces total DRAM access count by effectively utilizing the high temporal locality of R table. Discussed highlights of each optimization technique increase as the vector length grows larger, leading to more frequent ACTs within each bank group, creating an environment that allows bg-PIM to fully capitalize its parallelism.

The primary reason for relatively low speedup of HEAM-BG even though it utilizes bg-PIM is that the total embedding lookups in a single batch is small in critico dataset, resulting in low utilization of bg-PIM parallelism. The fact that baseline HBM2 is capable of embedding lookups of critico dataset due to its abundant channels further diminishes effect of HEAM-BG in this case. Coupled with the operation cycles of PIM and cycles required to deliver PIM instructions, this under-utilization issue especially gets worse for small vector length. However, when batching is applied, total embedding lookups per operation are increased, resulting in higher throughput than baseline.

6.2 Performance Evaluation with Previous NMP Designs

Speedup Comparison. To demonstrate the effectiveness of our proposal, we compare the overall performance of HEAM to the speedup in embedding operation of the previous works [6], [7], [8], [9]. In our experiment, total two DIMMs were utilized for previous DIMM based NMP architectures.

Through the use of HBM, 2-level PIM structure, and off-loading techniques, HEAM achieved the best speedup across all the prior works. Figure 10 shows the relative performance

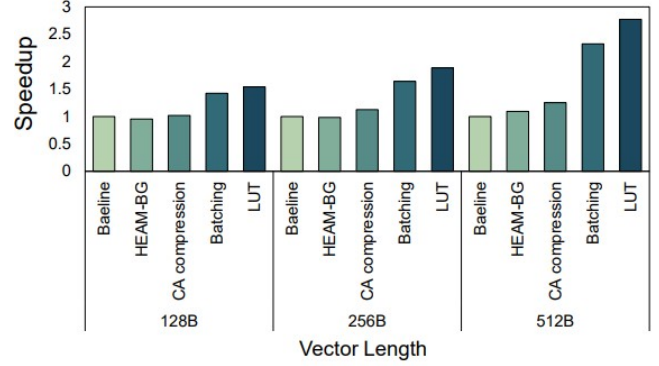


Figure 9. Performance Impact of Design Optimizations

of various configurations normalized to TensorDIMM, with varying vector lengths from 128B to 512B. Compared to the prior works, HEAM achieves 6.3 \times , 4.6 \times , 2.3 \times , 1.8 \times speedup compared to TensorDIMM, RecNMP, TRiM-G, SPACE when vector length is 512B. Compared to SPACE which also utilizes heterogeneous memory system, HEAM’s superior achievement in speedup comes from the utilization of bg-PIM followed by design choices of batching and LUT. The performance enhancement of HEAM increases as vector length gets larger, as internal bandwidth becomes more utilized due to more frequent ACTs occurring inside the memory. Larger pooling size and larger vector length, which is a normal trend of recommendation system in production, would result in even more enhancement.

Relative Energy Consumption. Figure 11 depicts the relative energy consumption of prior works and HEAM, which are normalized to the result of TensorDIMM. As shown in the figure, HEAM saves 58.9%, 45.9% and 14.1% energy compared to TensorDIMM, RecNMP and SPACE. HEAM saves 14.2% from SPACE energy consumption, similar to the amount of energy saved compared to TRiM-G.

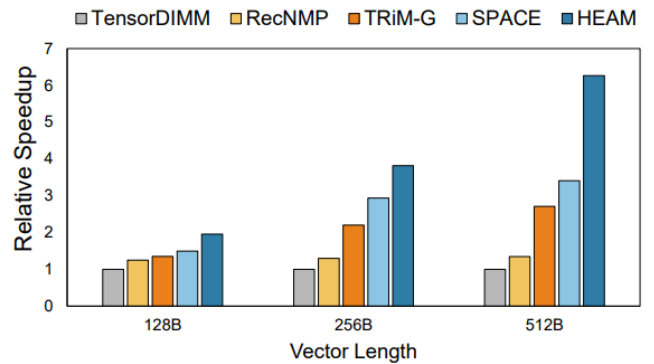


Figure 10. Performance evaluation on various NMP systems

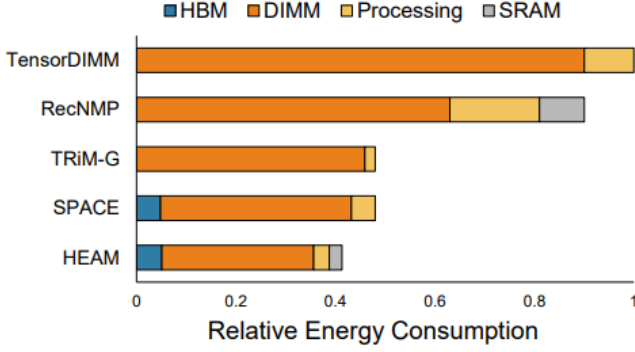


Figure 11. Relative energy consumption in NMP models

6.3 Design Overhead

The total area occupied by bg-PIM is 3.12mm^2 per each HBM2 die, which takes 3.44% portion of each HBM2 die. LUT consists of 20KB SRAM which takes 10% of the total PIM area. Each PIM includes four MAC units, register files for buffer and logic support. Total gate count is 118,087 per each bg-PIM. The energy consumption of LUT accounts for 0.04% from total energy consumed by HEAM which enables high energy savings from DRAM access.

6.4 Assessment of Compositional Embedding Shortcomings

Efficiency of Increasing Hash Collision. When the number of hash collisions increases, the decrease in the total number of hot vectors might not be directly proportional. Ideally, for a proportional reduction, hot vectors should be clustered so that a quotient hash function can map several hot vectors to a single one. However, due to the sparsity of hot vectors, such clustering is often not feasible. In the worst-case scenario, the reduction in the total number of hot q vectors is minimal, as each hot q vector is predominantly surrounded by cold vectors, leading to only a slight decrease from the original count. This minimal reduction in the total hot vectors, as hash collisions increase, presents a challenge in meeting the required bandwidth ratio between HBM and DIMM. For maximizing the bandwidth benefits, a significant reduction in the number of hot vectors that need to be offloaded to HBM is essential. However, if this reduction is only marginal despite an increase in hash collisions, achieving the desired bandwidth ratio becomes problematic.

To verify this impact, we measured the changes in the number of the hot vectors to the hot q vectors while modifying hash collision value on criteo-kaggle dataset [24], movielens-25M [31] and amazon electronics, which are public datasets that is available online. We defined hot vectors the vectors needed to achieve 80% of the cumulative request. The result is shown in Figure 12 (a). Although the result is not ideal, increasing hash collision produces decrease in hot vectors

that is enough to meet the bandwidth ratio demand between HBM and DIMM.

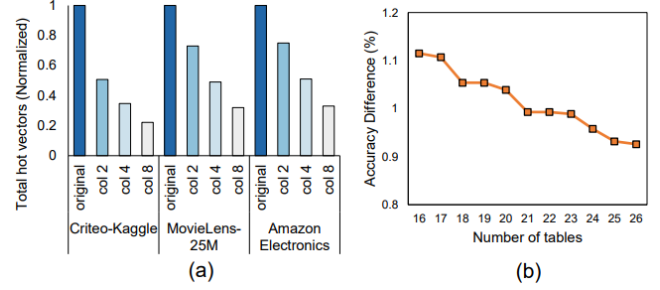


Figure 12. Compositional embedding shortcoming analysis. (a) Change in the number of hot vectors based on the hash collision value across criteo-kaggle, movielens-25M, amazon electronics. (b) Accuracy difference between the original model and the model trained with compositional embedding by hash collision 4.

Decrease in model quality drop with more embedding tables. As more embedding tables are being used in the recommendation system, the model quality increases [5]. In the production level, it is known that there are 10s of embedding tables. As the accuracy drop of compositional embedding is due to the mixture of distinctive embeddings [21], applying more embedding tables might resolve the accuracy drop caused when applying the algorithm. To see the effect of embedding tables on the accuracy, we conducted experiments in criteo-kaggle-dataset. Since some tables are used more often than others, we picked randomly the tables to be excluded, averaging the result of 3 experiments. The overall result is shown in Figure 12 (b). By excluding tables from 10 to 0, we found that the gap of accuracy drop decreases.

7 Conclusions

We introduce HEAM, a 3-level PIM architecture that comprises DIMM, HBM featuring bd-PIM and bg-PIM with LUT. Our goal is to accelerate compositional embedding. We have examined the distinct traits of compositional embedding and leveraged our findings to boost overall throughput. Our system tackles two key challenges in DLRM: model size expansion and memory-bound operations. In addition, HEAM effectively resolves the issue of double memory access that arises when applying compositional embedding, resulting in $6.3\times$ performance improvement and 58.9% energy savings compared to the previous NMP architectures tailored for recommendation system.

References

- [1] Maxim Naumov, Dheevatsa Mudigere, Hao-Jun Michael Shi, Jianyu Huang, Narayanan Sundaraman, Jongsoo Park, Xiaodong Wang, Udit

- Gupta, Carole-Jean Wu, Alisson G Azzolini, et al. Deep learning recommendation model for personalization and recommendation systems. *arXiv preprint arXiv:1906.00091*, 2019.
- [2] Paul Covington, Jay Adams, and Emre Sargin. Deep neural networks for youtube recommendations. In *Proceedings of the 10th ACM conference on recommender systems*, pages 191–198, 2016.
 - [3] Harald Steck, Linas Baltrunas, Ehtsham Elahi, Dawen Liang, Yves Raimond, and Justin Basilico. Deep learning for recommender systems: A netflix case study. *AI Magazine*, 42(3):7–18, 2021.
 - [4] Udit Gupta, Carole-Jean Wu, Xiaodong Wang, Maxim Naumov, Brandon Reagen, David Brooks, Bradford Cotel, Kim Hazelwood, Mark Hempstead, Bill Jia, et al. The architectural implications of facebook’s dnn-based personalized recommendation. In *2020 IEEE International Symposium on High Performance Computer Architecture (HPCA)*, pages 488–501. IEEE, 2020.
 - [5] Mark Zhao, Niket Agarwal, Aarti Basant, Buğra Gedik, Satadru Pan, Mustafa Ozdal, Rakesh Komuravelli, Jerry Pan, Tianshu Bao, Haowei Lu, et al. Understanding data storage and ingestion for large-scale deep recommendation model training: Industrial product. In *Proceedings of the 49th Annual International Symposium on Computer Architecture*, pages 1042–1057, 2022.
 - [6] Youngeun Kwon, Yunjae Lee, and Minsoo Rhu. Tensordimm: A practical near-memory processing architecture for embeddings and tensor operations in deep learning. In *Proceedings of the 52nd Annual IEEE/ACM International Symposium on Microarchitecture*, pages 740–753, 2019.
 - [7] Liu Ke, Udit Gupta, Benjamin Youngjae Cho, David Brooks, Vikas Chandra, Utku Diril, Amin Firoozshahian, Kim Hazelwood, Bill Jia, Hsien-Hsin S Lee, et al. Recnmp: Accelerating personalized recommendation with near-memory processing. In *2020 ACM/IEEE 47th Annual International Symposium on Computer Architecture (ISCA)*, pages 790–803. IEEE, 2020.
 - [8] Jaehyun Park, Byeongho Kim, Sungmin Yun, Eojin Lee, Minsoo Rhu, and Jung Ho Ahn. Trim: Enhancing processor-memory interfaces with scalable tensor reduction in memory. In *MICRO-54: 54th Annual IEEE/ACM International Symposium on Microarchitecture*, pages 268–281, 2021.
 - [9] Hongju Kal, Seokmin Lee, Gun Ko, and Won Woo Ro. Space: locality-aware processing in heterogeneous memory for personalized recommendations. In *2021 ACM/IEEE 48th Annual International Symposium on Computer Architecture (ISCA)*, pages 679–691. IEEE, 2021.
 - [10] Liu Ke, Xuan Zhang, Jinin So, Jong-Geon Lee, Shin-Haeng Kang, Sukhan Lee, Songyi Han, YeonGon Cho, Jin Hyun Kim, Yongsuk Kwon, et al. Near-memory processing in action: Accelerating personalized recommendation with axdim. *IEEE Micro*, 42(1):116–127, 2021.
 - [11] Bahar Asgari, Ramyad Hadidi, Jiasen Cao, Sung-Kyu Lim, Hyesoon Kim, et al. Fafnir: Accelerating sparse gathering by using efficient near-memory intelligent reduction. In *2021 IEEE International Symposium on High-Performance Computer Architecture (HPCA)*, pages 908–920. IEEE, 2021.
 - [12] Geet Sethi, Bilge Acun, Niket Agarwal, Christos Kozyrakis, Caroline Trippel, and Carole-Jean Wu. Recshard: statistical feature-based memory optimization for industry-scale neural recommendation. In *Proceedings of the 27th ACM International Conference on Architectural Support for Programming Languages and Operating Systems*, pages 344–358, 2022.
 - [13] Dheevatsa Mudigere, Yuchen Hao, Jianyu Huang, Zhihao Jia, Andrew Tulloch, Srinivas Sridharan, Xing Liu, Mustafa Ozdal, Jade Nie, Jongsoo Park, et al. Software-hardware co-design for fast and scalable training of deep learning recommendation models. In *Proceedings of the 49th Annual International Symposium on Computer Architecture*, pages 993–1011, 2022.
 - [14] Ehsan K Ardestani, Changkyu Kim, Seung Jae Lee, Luoshang Pan, Jens Axboe, Valmiki Rampersad, Banit Agrawal, Fuxun Yu, Ansha Yu, Trung Le, et al. Supporting massive dlrn inference through software defined memory. In *2022 IEEE 42nd International Conference on Distributed Computing Systems (ICDCS)*, pages 302–312. IEEE, 2022.
 - [15] Liu Ke, Udit Gupta, Mark Hempstead, Carole-Jean Wu, Hsien-Hsin S Lee, and Xuan Zhang. Hercules: Heterogeneity-aware inference serving for at-scale personalized recommendation. In *2022 IEEE International Symposium on High-Performance Computer Architecture (HPCA)*, pages 141–154. IEEE, 2022.
 - [16] Amin Firoozshahian, Joel Coburn, Roman Levenstein, Rakesh Nattoji, Ashwin Kamath, Olivia Wu, Gurdeepak Grewal, Harish Aepala, Bhasker Jakka, Bob Dreyer, et al. Mtia: First generation silicon targeting meta’s recommendation systems. In *Proceedings of the 50th Annual International Symposium on Computer Architecture*, pages 1–13, 2023.
 - [17] Weijie Zhao, Jingyuan Zhang, Deping Xie, Yulei Qian, Ronglai Jia, and Ping Li. Aibox: Ctr prediction model training on a single node. In *Proceedings of the 28th ACM International Conference on Information and Knowledge Management*, pages 319–328, 2019.
 - [18] Hao-Jun Michael Shi, Dheevatsa Mudigere, Maxim Naumov, and Jiyan Yang. Compositional embeddings using complementary partitions for memory-efficient recommendation systems. In *Proceedings of the 26th ACM SIGKDD International Conference on Knowledge Discovery & Data Mining*, pages 165–175, 2020.
 - [19] Antonio A Ginart, Maxim Naumov, Dheevatsa Mudigere, Jiyan Yang, and James Zou. Mixed dimension embeddings with application to memory-efficient recommendation systems. In *2021 IEEE International Symposium on Information Theory (ISIT)*, pages 2786–2791. IEEE, 2021.
 - [20] Chunxing Yin, Bilge Acun, Carole-Jean Wu, and Xing Liu. Tt-rec: Tensor train compression for deep learning recommendation models. *Proceedings of Machine Learning and Systems*, 3:448–462, 2021.
 - [21] Fuyuan Lyu, Xing Tang, Hong Zhu, Huifeng Guo, Yingxue Zhang, Ruiming Tang, and Xue Liu. Optembed: Learning optimal embedding table for click-through rate prediction. In *Proceedings of the 31st ACM International Conference on Information & Knowledge Management*, pages 1399–1409, 2022.
 - [22] Kilian Weinberger, Anirban Dasgupta, John Langford, Alex Smola, and Josh Attenberg. Feature hashing for large scale multitask learning. In *Proceedings of the 26th annual international conference on machine learning*, pages 1113–1120, 2009.
 - [23] Wang-Cheng Kang, Derek Zhiyuan Cheng, Tiansheng Yao, Xinyang Yi, Ting Chen, Lichan Hong, and Ed H Chi. Learning to embed categorical features without embedding tables for recommendation. In *Proceedings of the 27th ACM SIGKDD Conference on Knowledge Discovery & Data Mining*, pages 840–850, 2021.
 - [24] CriteoLabs. 2014. Kaggle display advertising challenge dataset. <https://jmcauley.ucsd.edu/data/amazon/>.
 - [25] Vijay Janapa Reddi, Christine Cheng, David Kanter, Peter Mattson, Guenther Schmuelling, Carole-Jean Wu, Brian Anderson, Maximilien Breughe, Mark Charlebois, William Chou, et al. Mlperf inference benchmark. In *2020 ACM/IEEE 47th Annual International Symposium on Computer Architecture (ISCA)*, pages 446–459. IEEE, 2020.
 - [26] Shang Li, Zhiyuan Yang, Dhiraj Reddy, Ankur Srivastava, and Bruce Jacob. Drsim3: A cycle-accurate, thermal-capable dram simulator. *IEEE Computer Architecture Letters*, 19(2):106–109, 2020.
 - [27] Jaewoong Sim, Alaa R Alameldeen, Zeshan Chishti, Chris Wilkerson, and Hyesoon Kim. Transparent hardware management of stacked dram as part of memory. In *2014 47th Annual IEEE/ACM International Symposium on Microarchitecture*, pages 13–24. IEEE, 2014.
 - [28] Chia Chen Chou, Aamer Jaleel, and Moinuddin K Qureshi. Cameo: A two-level memory organization with capacity of main memory and flexibility of hardware-managed cache. In *2014 47th Annual IEEE/ACM International Symposium on Microarchitecture*, pages 1–12. IEEE, 2014.
 - [29] Chiachen Chou, Aamer Jaleel, and Moinuddin K Qureshi. Bear: Techniques for mitigating bandwidth bloat in gigascale dram caches. *ACM SIGARCH Computer Architecture News*, 43(35):198–210, 2015.

- [30] Naveen Muralimanohar, Rajeev Balasubramonian, and Norman P Jouppi. Cacti 6.0: A tool to model large caches. *HP laboratories*, 27:28, 2009.
- [31] movielens. 2019. Movielens 25m dataset. <https://grouplens.org/datasets/movielens/25m/>.